ChemComm

COMMUNICATION

View Article Online
View Journal | View Issue

Cite this: *Chem. Commun.*, 2023, **59**, 12302

Received 21st August 2023,
Accepted 19th September 2023

DOI: 10.1039/d3cc04012g

rsc.li/chemcomm

A narrow-band deep-blue MRTADF-type organic afterglow emitter†

Guangming Wang,‡ Shuhui Ding,‡ Jiuyang Li,‡ Zi Ye, Wen Xia, Xuefeng Chen and Kaka Zhang *

We report a multi-resonant thermally activated delayed fluorescent (MRTADF) afterglow emitter with unprecedented long emission lifetime > 100 ms, full-width at half-maximum < 40 nm, and deep-blue emission color of CIEy at 0.048. Such emitters remain rarely achieved and would show potential applications in multiplexed bioimaging and high-density information encryption.

Room-temperature phosphorescence (RTP) and organic afterglow materials feature long-lived excited states[1–10] and display applications in high-contrast bioimaging (negligible background fluorescence in time-gated imaging mode),[11–13] oxygen sensing and mapping (based on organic triplets' sensitivity towards molecular oxygen),[14–16] and advanced anticounterfeiting and information encryption (on the basis of afterglow patterns/colours and their changes after ceasing excitation source).[17–20] It has been reported that multiplexed bioimaging requires the use of narrow-band luminescent probes to minimize spectral crosstalk.[21–23] In the aspect of optical anticounterfeiting and information encryption, the realization of high-density information storage relies on narrow-band emitters to address the issue of "spectral crowding".[24–26] However, despite the tremendous development of the field of organic afterglow materials in the past decade,[1–20] most of the reported afterglow emitters exhibit broad emission bands with full-width at half-maximum (FWHM) larger than 50 nm and even around 100 nm. Such emission spectral broadening is mainly caused by two factors: (1) vibronic coupling between excited states and ground states; (2) structural relaxation of excited states.

The multiple resonance effect has been reported to enable the localization of the HOMO and LUMO on different atoms, reduce the vibronic coupling and consequently narrow the emission spectra.[27–32] Recent studies have shown that multi-resonant thermally activated delayed fluorescent (MRTADF) emitters serve as promising candidates for developing high-quality and energy-saving OLED displays. It is noteworthy that such MRTADF emitters of narrow-band emission possess reverse intersystem crossing rate (k_{RISC}) of 10^3 to 10^6 s^{-1}.[27–32] It is well known that large k_{RISC} is required to avoid efficiency roll off of OLED displays at relatively high luminance. However, large k_{RISC} of 10^3 to 10^6 s^{-1} means short delayed fluorescence lifetimes of 10^{-6} to 10^{-3} s, which is detrimental to the fabrication of afterglow materials with emission lifetimes longer than 100 ms. Recent studies on TADF-type organic afterglow by us and others reveal that the requirement of k_{RISC} in afterglow material design is the opposite to that in OLED display fabrication; moderate k_{RISC} of 10^{-1} to 10^1 s^{-1} is favored for the design of TADF-type afterglow materials.[33–38] Probably because of this, despite the fact that many narrow-band MRTADF emitters for OLEDs have been reported, MRTADF-type organic afterglow materials with emission lifetimes ≥ 100 ms and narrow-band emission remain rarely explored.

The key to achieving narrow-band MRTADF-type organic afterglow is to use a MRTADF emitter featuring moderate k_{RISC} of 10^{-1} to 10^1 s^{-1}, which is a prerequisite for the realization of long emission lifetimes ⩾ 100 ms. Given that most organic systems in the absence of heavy atom effects and benzophenone functional groups possess phosphorescence rates (k_P) of 10^{-2}–10^2 s^{-1}, such moderate k_{RISC} is sufficient to open the TADF pathway for converting organic triplets into singlets. Another key point is the employment of suitable crystalline or glassy matrices to reduce organic triplets' nonradiative decay rate (k_{nr}) and oxygen quenching rate (k_q) to small values < k_{RISC}.[39–43]

Here we report the emergence of MRTADF-type organic afterglow *via* doping 10-phenylacridone (compound **1**) into a phenyl benzoate (PhB) matrix (Fig. 1a). The resultant afterglow materials exhibit narrow-band emission with FWHM of 38 nm, deep-blue emission color of CIEy at 0.048, and long emission lifetime of 0.2 s. By incorporating **1** into the emulsion

Key Laboratory of Synthetic and Self-Assembly Chemistry for Organic Functional Molecules, Shanghai Institute of Organic Chemistry, University of Chinese Academy of Sciences, Chinese Academy of Sciences, 345 Lingling Road, Shanghai 200032, People's Republic of China. E-mail: zhangkaka@sioc.ac.cn

† Electronic supplementary information (ESI) available: Experimental procedures, and spectroscopic data. See DOI: https://doi.org/10.1039/d3cc04012g

‡ Equal contribution.

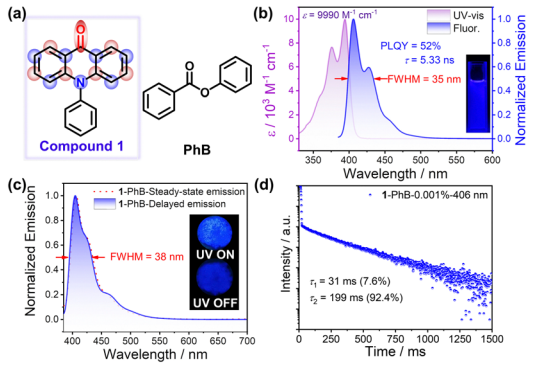

Fig. 1 (a) Structure of **1** and PhB. (b) UV-vis absorption (not normalized) and steady-state emission spectra (36.8 μM, excited at 365 nm) of **1** in dichloromethane. (c) Room-temperature steady-state and delayed emission spectra (1 ms delay) and (d) emission decay (monitored at 406 nm) of the **1**-PhB-0.001% solid sample excited at 365 nm.

polymerization system, narrow-band deep-blue aqueous afterglow dispersion can be obtained, displaying promising applications.

Compound **1** (purchased from Leyan Company, Shanghai) was purified by recrystallization in spectroscopic grade dichloromethane/*n*-hexane. Its high purity was confirmed by HPLC (Fig. S1, ESI†). The solution of **1** in dichloromethane exhibits a UV-vis absorption maximum at 394 nm (ε = 9.99 × 10^3 M^{-1} cm^{-1}) and deep-blue emission (under 365 nm UV lamp) with λ_{em} at 406 nm (FWHM, 35 nm; τ_F, 5.33 ns) and photoluminescence quantum yield (PLQY) of 52% (Fig. 1b and Fig. S2, ESI†). The absorption and fluorescence spectra obey the mirror image rule (Fig. 1b), with small Stokes shift of 750 cm^{-1} estimated from spectral maxima.

Single-component **1** samples don't show room-temperature afterglow either in solution or the solid state (Fig. S3, ESI†). Recent studies by us and others have demonstrated that, in two-component afterglow systems, suitable organic matrices assist luminescent dopants' intersystem crossing (ISC) and protect dopants' triplet excited states from nonradiative decay and oxygen quenching.[33–36] PhB crystalline matrices, which also don't show room-temperature afterglow (Fig. S4, ESI†), have a melting point of around 70 °C and thus can protect dopants' triplets by the rigid environment at room temperature.[40,42] PhB has a high T_1 level (approximately 3.4 eV estimated by TD-DFT, Text S1, ESI†), which can resist excited state energy transfer from dopant to matrix and subsequent afterglow quenching.[39,44] Upon doping 0.001 wt% **1** into PhB, the resultant **1**-PhB-0.001% solid sample exhibits deep-blue afterglow under ambient conditions (Fig. 1c). Room-temperature delayed emission spectra (1 ms delay, excited at 365 nm) show narrow emission band at 406 nm with CIE coordinates (0.158, 0.048) and small FWHM of 38 nm (Fig. 1c and Fig. S5 and Text S2, ESI†). The PLQY of the **1**-PhB-0.001% sample has been measured to be 19.4%. The emission lifetime can be fit into double-exponential decay with τ_1 = 31 ms (7.6%) and τ_2 = 199 ms (92.4%) (Fig. 1d), where the τ_2 part is responsible for the deep-blue afterglow. The **1**-PhB-0.01% sample has similar photophysical properties (Fig. S6, ESI†) to the **1**-PhB-0.001% sample. Other matrices such as benzoic acid, boric acid, and 4-methoxybenzophenone were tested, but the resultant **1**-matrix samples showed weak room-temperature afterglow and the afterglow color is cyan rather than deep-blue (Fig. S7, ESI†).

It is noteworthy that the steady-state emission spectra of the **1**-PhB-0.001% sample almost coincide with the delayed emission spectra (excited at 365 nm, Fig. 1c). In the literature, there are only several instances exhibiting the coincidence of steady-state and delayed emission spectra. (1) Excited state energy transfer from the afterglow donor to the fluorescence acceptor can give rise to spectral coincidence,[45] which only occurs when the afterglow donor is sufficiently excited. PhB matrices show no absorption at 365 nm (Fig. S4, ESI†), so the energy transfer mechanism is not the case here. (2) Intermolecular charge transfer and retarded charge recombination in donor–acceptor systems have been reported to show organic long persistent luminescence (OLPL) with identical steady-state and delayed emission spectra.[46] The PhB matrix has a low-lying HOMO (−6.43 eV, Fig. S8, ESI†) and high-lying LUMO (−2.01 eV) compared to **1** (−5.53 eV and −2.61 eV, Fig. S9, ESI†), so the OLPL mechanism should be absent here. (3) Organic systems with strong ISC, such as the benzophenone system, would exhibit identical steady-state and delayed emission spectra.[42,47] This is not the case here, as revealed by variable temperature delayed emission spectra (*vide infra*). (4) The impurity mechanism may give spectral coincidence between the steady-state and delayed emission spectra.[48] Here **1** has high purity as confirmed by HPLC (Fig. S1, ESI†). **1** and PhB matrices don't show room-temperature afterglow (Fig. S3 and S4, ESI†). Besides, the excitation spectra of the **1**-PhB-0.001% sample exhibit similar maxima to **1**'s UV-vis absorption spectra (Fig. S10, ESI†). The UV-vis spectra show an electronic absorption property of **1**, while excitation spectra reveal the absorption property of the luminescent component in the system. The match between the UV-vis and excitation spectra suggests that the luminescent property originates from **1** rather than impurities. Moreover, the mirror image of the UV-vis and emission spectra in the **1** system also support that the luminescent property here is exclusively from **1** dispersed in PhB matrices.

To further investigate the afterglow mechanism, variable temperature delayed emission spectra (1 ms delay) have been collected (Fig. 2a). At 77 K, the **1**-PhB-0.001% sample shows bluish green afterglow (Fig. 2a and Fig. S11, ESI†), and the

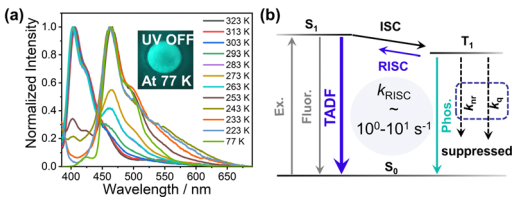

Fig. 2 (a) Variable temperature delayed emission spectra (1 ms delay) of the **1**-PhB-0.001% sample. The inset shows its afterglow photograph at 77 K. (b) Proposed TADF afterglow mechanism of the **1**-PhB-0.001% sample.

delayed emission band at 464 nm can be assigned as phosphorescence decay of **1**'s triplets; the T_1 level was obtained from the phosphorescence maximum to be 2.67 eV. The phosphorescence decay rate (k_P) was estimated from the phosphorescence lifetime (837 ms, Fig. S12, ESI†) to be 1.2 s^{-1}. By increasing the temperature, the delayed fluorescence band at 406 nm (S_1 level, 3.05 eV) increases and then dominates the whole delayed emission spectra at 293 K and higher temperature (Fig. 2a). The delayed fluorescence is exclusively attributed to thermally activated delayed fluorescence (TADF), since triplet–triplet annihilation (TTA that can also give rise to delayed fluorescence) should be absent at such low doping concentration of 0.001 wt%.[49] Based on temperature-dependent emission decay, the Arrhenius plot of the k_{RISC} gives an experimental ΔE_{ST} of 0.39 eV (Fig. S13, ESI†), which agrees with the experimental results obtained from fluorescence and phosphorescence maxima (0.38 eV). Power-dependent delayed emission spectra at room temperature (Fig. S14, ESI†) show a quasi-linear relationship between delayed fluorescence intensity and excitation power further confirming the TADF-type afterglow mechanism. The **1**-PhB-0.001% sample under ambient conditions exhibits τ_1 = 31 ms (7.6%) and τ_2 = 199 ms (92.4%), as shown in Fig. 1d. The τ_1 part, which is largely overestimated,[50] originates from prompt fluorescence and the accurate value has been obtained by a picosecond pulse laser to be 3.36 ns (Fig. S15, ESI†). The τ_2 part originates from TADF afterglow, from which k_{RISC} was roughly estimated to be 10^0–10^1 s^{-1}. The rigid crystalline PhB matrices, as well as intermolecular interaction between **1** and PhB, efficiently protect **1**'s triplets from quenching. With the suppressed k_{nr} and k_q, the moderate k_{RISC} can explain the emergence of TADF afterglow with 0.2 s lifetime under ambient conditions (Fig. 2b).

Conventional TADF emitters with ΔE_{ST} of around 0.2 eV or lower for OLEDs usually possess k_{RISC} of 10^3 to 10^6 s^{-1}. It has been reported that the increase of ΔE_{ST} by 0.1 eV would result in the decrease of k_{RISC} by approximately 100-fold.[51] Here, the moderate ΔE_{ST} value (0.38 eV) agrees with the observation of TADF-type afterglow with moderate k_{RISC} of 10^0–10^1 s^{-1} under ambient conditions. To gain a further insight, we conduct a theoretical investigation (Tables S1–S8, ESI†). **1** in dichloromethane was simulated utilizing the polarizable continuum model (PCM). The geometry structures and frequency analyses of the ground and excited states of **1** have been obtained by DFT and TD-DFT methods, employing the TPSSh functional and the 6-31+G(d,p) basis set.[52] For ISC, the electronic energies and spin–orbit coupling matrix elements (SOCMEs) have been calculated by the ORCA 5.0.3 program with spin–orbit mean-field methods at the STEOM-DLPNO-CCSD/def2-TZVP theoretical level based on the optimized geometries. Using the simplified formula proposed by Kaji and coworkers,[52,53] the fluorescence decay rate of the S_1 state (k_F) is calculated to be 3.05×10^8 s^{-1} (Table S5, ESI†), which is consistent with the experimental result (0.97×10^8 s^{-1}) in dichloromethane. The S_1-to-T_1 ISC rate is calculated by Marcus theory to be 1.19×10^7 s^{-1}, which allows the population of **1**'s triplets. According to our previous study,[33–36] PhB matrices can also assist the population of dopants' triplets *via* dipole–dipole interactions (PhB's ground state dipole moment, 2.02 debye; **1**'s S_1 state dipole moment, 17.36 debye; Fig. S16, ESI†). k_{RISC} at 300 K is calculated by Marcus theory to be 6.62 s^{-1}, which also agrees with experimental observations. Given that the experimental k_P is 1.2 s^{-1}, such k_{RISC} is enough to enable TADF-type afterglow with emission lifetime > 100 ms under ambient conditions where the nonradiative decay and oxygen quenching of **1**'s triplets are suppressed in the rigid PhB matrices.

The narrow-band emission of the **1**-PhB-0.001% sample can be attributed to the multiple resonance effect of the nitrogen atom and carbonyl group on compound **1** (Fig. 1a); such arrangement reduces vibronic coupling between the excited states and ground states (Fig. S9, ESI†).[27–32] Besides, the relatively rigid structure of compound **1** restricts structural relaxation of the excited states, which can also narrow the emission band (Text S2, ESI†). Narrow-band MRTADF-type organic afterglow materials with emission lifetime > 100 ms have been rarely reported in the literature, despite the fact that many narrow-band MRTADF emitters (with emission lifetime of 10^{-6} to 10^{-3} s) have been developed for OLED devices.

To explore the function of the present MRTADF afterglow system, we prepare aqueous afterglow dispersions in view of their promising biomedical applications.[12–16] Most of the reported methods for aqueous afterglow material fabrication are based on mechanical processing of solid-state afterglow materials, which would disrupt the rigid environment for the protection of organic triplets and cause a drastic loss of afterglow performance. Here, we introduce **1** into the emulsion polymerization system to prepare an aqueous afterglow dispersion (experimental details in the ESI†).[54,55] The resultant **1**-PMMA emulsion inherits the narrow-band deep-blue MRTADF-type organic afterglow property of **1**, exhibiting a delayed emission band at 409 nm with FWHM of 40 nm at room temperature (Fig. 3a). The emission lifetime of the **1**-PMMA emulsion can be fit into double-exponential decay with τ_1 = 78 ms (19.5%) and τ_2 = 400 ms (80.5%) (Fig. 3b); glassy

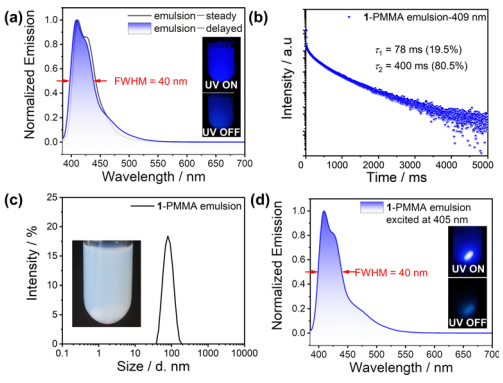

Fig. 3 (a) Room-temperature steady-state and delayed emission spectra (1 ms delay) and (b) emission decay curve (monitored at 409 nm) of the **1**-PMMA emulsion excited at 365 nm. (c) Hydrodynamic diameter distribution of the **1**-PMMA emulsion estimated by DLS. (d) Room-temperature delayed emission spectra (1 ms delay) of the **1**-PMMA emulsion excited at 405 nm.

PMMA latex protect **1**'s triplets. Dynamic light-scattering (DLS) measurement shows that the average hydrodynamic diameter of the **1**-PMMA emulsion is 78 nm with a polydispersity index of 0.058 (Fig. 3c). Given the small Stokes shift of compound **1**, we use 405 nm visible light to excite the **1**-PMMA emulsion. The afterglow photograph shown in Fig. 3d and delayed emission spectra (excited at 405 nm) demonstrate the visible-light-excitable property of the **1**-PMMA emulsion with a deep-blue afterglow band at 409 nm and FWHM of 40 nm (Fig. 3d). Such MRTADF afterglow emulsion in an aqueous medium would display potential bioimaging applications.

In summary, we achieve narrow-band deep-blue MRTADF-type organic afterglow by doping **1** into small organic crystalline matrices or glassy PMMA emulsion latex. These MRTADF afterglow materials possess emission lifetimes longer than 100 ms, which is among the highest values in the reported MRTADF emitters. In the field of organic afterglow materials, narrow-band MRTADF afterglow materials have been rarely reported, which would show potential applications in multiplexed bioimaging and high-density information encryption.

We thank the National Natural Science Foundation of China (22175194), Hundred Talents Program from Shanghai Institute of Organic Chemistry (Y121078), and Pioneer Hundred Talents Program of Chinese Academy of Sciences (E320021).

Conflicts of interest

There are no conflicts to declare.

Notes and references

1 V. W.-W. Yam, V. K.-M. Au and S. Y.-L. Leung, *Chem. Rev.*, 2015, **115**, 7589–7728.
2 W. Zhao, Z. He and B. Z. Tang, *Nat. Rev. Mater.*, 2020, **5**, 869–885.
3 N. Gan, H. Shi, Z. An and W. Huang, *Adv. Funct. Mater.*, 2018, **28**, 1802657.
4 X. Ma, J. Wang and H. Tian, *Acc. Chem. Res.*, 2019, **52**, 738–748.
5 S. Hirata, *Adv. Opt. Mater.*, 2017, **5**, 1700116.
6 Kenry, C. Chen and B. Liu, *Nat. Commun.*, 2019, **10**, 2111.
7 Q. Li and Z. Li, *Acc. Chem. Res.*, 2020, **53**, 962–973.
8 J. Guo, C. Yang and Y. Zhao, *Acc. Chem. Res.*, 2022, **55**, 1160–1170.
9 H. Nie, Z. Wei, X.-L. Ni and Y. Liu, *Chem. Rev.*, 2022, **122**, 9032–9077.
10 A. Forni, E. Lucenti, C. Botta and E. Cariati, *J. Mater. Chem. C*, 2018, **6**, 4603–4626.
11 X. Zhen, Y. Tao, Z. An, P. Chen, C. Xu, R. Chen, W. Huang and K. Pu, *Adv. Mater.*, 2017, **29**, 1606665.
12 X.-F. Wang, H. Xiao, P.-Z. Chen, Q.-Z. Yang, B. Chen, C.-H. Tung, Y.-Z. Chen and L.-Z. Wu, *J. Am. Chem. Soc.*, 2019, **141**, 5045–5050.
13 Y. Wang, H. Gao, J. Yang, M. Fang, D. Ding, B. Z. Tang and Z. Li, *Adv. Mater.*, 2021, **33**, 2007811.
14 G. Zhang, G. M. Palmer, M. W. Dewhirst and C. L. Fraser, *Nat. Mater.*, 2009, **8**, 747–751.
15 Y. Yu, M. S. Kwon, J. Jung, Y. Zeng, M. Kim, K. Chung, J. Gierschner, J. H. Youk, S. M. Borisov and J. Kim, *Angew. Chem., Int. Ed.*, 2017, **56**, 16207–16211.
16 Y. Zhou, W. Qin, C. Du, H. Gao, F. Zhu and G. Liang, *Angew. Chem., Int. Ed.*, 2019, **58**, 12102–12106.
17 Z. An, C. Zheng, Y. Tao, R. Chen, H. Shi, T. Chen, Z. Wang, H. Li, R. Deng, X. Liu and W. Huang, *Nat. Mater.*, 2015, **14**, 685–690.
18 X. Yan, H. Peng, Y. Xiang, J. Wang, L. Yu, Y. Tao, H. Li, W. Huang and R. Chen, *Small*, 2022, **18**, 2104073.
19 X. Yu, H. Zhang and J. Yu, *Aggregate*, 2021, **2**, 20–34.
20 Z. He, H. Gao, S. Zhang, S. Zheng, Y. Wang, Z. Zhao, D. Ding, B. Yang, Y. Zhang and W. Z. Yuan, *Adv. Mater.*, 2019, **31**, 1807222.
21 J. Han, A. Xia, Y. Huang, L. Ni, W. Chen, Z. Jin, S. Yang and F. Jin, *ACS Synth. Biol.*, 2019, **8**, 2536–2546.
22 M. Li, S. Tian, F. Meng, M. Yin, Q. Yue, S. Wang, W. Bu and L. Luo, *Nano Lett.*, 2022, **22**, 4544–4551.
23 I. L. Medintz, H. T. Uyeda, E. R. Goldman and H. Mattoussi, *Nat. Mater.*, 2005, **4**, 435–446.
24 Y. Lei, W. Dai, J. Guan, S. Guo, F. Ren, Y. Zhou, J. Shi, B. Tong, Z. Cai, J. Zheng and Y. Dong, *Angew. Chem., Int. Ed.*, 2020, **59**, 16054–16060.
25 L. Lei, Y. Wang, W. Xu, R. Ye, Y. Hua, D. Deng, L. Chen, P. N. Prasad and S. Xu, *Nat. Commun.*, 2022, **13**, 5739.
26 Y. Su, Y. Zhang, Z. Wang, W. Gao, P. Jia, D. Zhang, C. Yang, Y. Li and Y. Zhao, *Angew. Chem., Int. Ed.*, 2020, **59**, 9967–9971.
27 T. Hatakeyama, K. Shiren, K. Nakajima, S. Nomura, S. Nakatsuka, K. Kinoshita, J. Ni, Y. Ono and T. Ikuta, *Adv. Mater.*, 2016, **28**, 2777–2781.
28 Y. Kondo, K. Yoshiura, S. Kitera, H. Nishi, S. Oda, H. Gotoh, Y. Sasada, M. Yanai and T. Hatakeyama, *Nat. Photonics*, 2019, **13**, 678–682.
29 J. M. Ha, S. H. Hur, A. Pathak, J.-E. Jeong and H. Y. Woo, *NPG Asia Mater.*, 2021, **13**, 53.
30 Y. Zhang, D. Zhang, J. Wei, Z. Liu, Y. Lu and L. Duan, *Angew. Chem., Int. Ed.*, 2019, **58**, 16912–16917.
31 T. Wang, X. Yin, X. Cao and C. Yang, *Angew. Chem., Int. Ed.*, 2023, **62**, e202301988.
32 X. Wu, B.-K. Su, D.-G. Chen, D. Liu, C.-C. Wu, Z.-X. Huang, T.-C. Lin, C.-H. Wu, M. Zhu, E. Y. Li, W.-Y. Hung, W. Zhu and P.-T. Chou, *Nat. Photonics*, 2021, **15**, 780–786.
33 X. Wang, Y. Sun, G. Wang, J. Li, X. Li and K. Zhang, *Angew. Chem., Int. Ed.*, 2021, **60**, 17138–17147.
34 Y. Pan, J. Li, X. Wang, Y. Sun, J. Li, B. Wang and K. Zhang, *Adv. Funct. Mater.*, 2022, **32**, 2110207.
35 G. Wang, J. Li, X. Li, X. Wang, Y. Sun, J. Liu and K. Zhang, *Chem. Eng. J.*, 2022, **431**, 134197.
36 G. Wang, X. Chen, J. Liu, S. Ding and K. Zhang, *Sci. China: Chem.*, 2023, **66**, 1120–1131.
37 Y. Liang, C. Xu, H. Zhang, S. Wu, J. Li, Y. Yang, Z. Mao, S. Luo, C. Liu, G. Shi, F. Sun, Z. Chi and B. Xu, *Angew. Chem., Int. Ed.*, 2023, **62**, e202217616.
38 J. Wang, Y. Yang, K. Li, L. Zhang and Z. Li, *Angew. Chem., Int. Ed.*, 2023, **62**, e202304020.
39 S. Hirata, K. Totani, J. Zhang, T. Yamashita, H. Kaji, S. R. Marder, T. Watanabe and C. Adachi, *Adv. Funct. Mater.*, 2013, **23**, 3386–3397.
40 J. Li, X. Wang, Y. Pan, Y. Sun, G. Wang and K. Zhang, *Chem. Commun.*, 2021, **57**, 8794–8797.
41 X. Chen, G. Wang, X. Chen, X. Deng and K. Zhang, *J. Mater. Chem. C*, 2022, **10**, 11634–11641.
42 Y. Su, M. Wu, G. Wang, J. Li, X. Chen, X. Li, G. Wang and K. Zhang, *Chem. Commun.*, 2023, **59**, 1525–1528.
43 S. Guo, W. Dai, X. Chen, Y. Lei, J. Shi, B. Tong, Z. Cai and Y. Dong, *ACS Mater. Lett.*, 2021, **3**, 379–397.
44 N. Notsuka, R. Kabe, K. Goushi and C. Adachi, *Adv. Funct. Mater.*, 2017, **27**, 1703902.
45 S. Kuila and S. J. George, *Angew. Chem., Int. Ed.*, 2020, **59**, 9393–9397.
46 R. Kabe and C. Adachi, *Nature*, 2017, **550**, 384–387.
47 W. Z. Yuan, X. Y. Shen, H. Zhao, J. W. Y. Lam, L. Tang, P. Lu, C. Wang, Y. Liu, Z. Wang, Q. Zheng, J. Z. Sun, Y. Ma and B. Z. Tang, *J. Phys. Chem. C*, 2010, **114**, 6090–6099.
48 C. Chen, Z. Chi, K. C. Chong, A. S. Batsanov, Z. Yang, Z. Mao, Z. Yang and B. Liu, *Nat. Mater.*, 2021, **20**, 175–180.
49 Z. Lin, R. Kabe, K. Wang and C. Adachi, *Nat. Commun.*, 2020, **11**, 191.
50 H. Noda, H. Nakanotani and C. Adachi, *Chem. Lett.*, 2019, **48**, 126–129.
51 P. K. Samanta, D. Kim, V. Coropceanu and J.-L. Brédas, *J. Am. Chem. Soc.*, 2017, **139**, 4042–4051.
52 K. Shizu and H. Kaji, *Commun. Chem.*, 2022, **5**, 53.
53 K. Shizu and H. Kaji, *J. Phys. Chem. A*, 2021, **125**, 9000–9010.
54 J. Liu, Y. Sun, G. Wang, X. Chen, J. Li, X. Wang, Y. Zou, B. Wang and K. Zhang, *Adv. Opt. Mater.*, 2022, **10**, 2201502.
55 X. Zhai, Y. Zeng, X. Deng, Q. Lou, A. Cao, L. Ji, Q. Yan, B. Wang and K. Zhang, *Chem. Commun.*, 2023, **59**, 10500–10503.